Impact of Siberian forest fires on the atmosphere over the Korean Peninsula during summer 2014

Jinsang Jung[a,*], Youngsook Lyu[b], Minhee Lee[b], Taekyung Hwang[b], Sangil Lee[a], Sanghyub Oh[a]

[a]Center for Gas Analysis, Korea Research Institute of Standards and Science (KRISS), Daejeon 34113, Republic of Korea

[b]Department of Climate and Air Quality Research, National Institute of Environmental Research, Daejeon 34944, Republic of Korea

Running title: Russian Forest Fire

Last modified: May 06, 2016

To be submitted to *Atmospheric Chemistry and Physics*

*Corresponding author: Jinsang Jung (jsjung@kriss.re.kr)

Abstract

Extensive forest fires occurred during late July 2014 across the forested region of Siberia, Russia. Smoke plumes emitted from Siberian forest fires underwent long-range transport over Mongolia and northeast China to the Korean Peninsula, which is located ~3000 km south of the Siberian forest. A notably high aerosol optical depth of ~4 was observed at a wavelength of 500 nm near the source of the Siberian forest fires. Smoke plumes reached 3–5 km in height near the source and fell below 2 km over the Korean Peninsula. Elevated concentrations of levoglucosan were observed (119.7 ± 6.0 ng m^{-3}), which were ~4.5 times higher than those observed during non-event periods in July 2014. During the middle of July 2014, a haze episode occurred that was primarily caused by the long-range transport of emission plumes originating from urban and industrial complexes in East China. Sharp increases in SO_4^{2-} concentrations (to 23.1 ± 2.1 μg m^{-3}) were observed during this episode. The haze caused by the long-range transport of Siberian forest fire emissions was clearly identified by relatively high organic carbon (OC)/elemental carbon (EC) ratios (7.18 ± 0.2) and OC/SO_4^{2-} ratios (1.31 ± 0.07) compared with those of the Chinese haze episode (OC/EC ratio: 2.4 ± 0.4; OC/SO_4^{2-} ratio: 0.21 ± 0.05). Remote measurement techniques and chemical analyses of the haze plumes clearly show that the haze episode that occurred during late July 2014 was caused mainly by the long-range transport of smoke plumes emitted from Siberian forest fires.

1. Introduction

Forest fires emit large amounts of gaseous and particulate pollutants into the atmosphere, including carbon dioxide (CO_2), carbon monoxide (CO), methane (CH_4), nitrogen oxides (NO_x), ammonia (NH_3), particulate matter (PM), non-methane hydrocarbon (NMHC), and other chemical species (Crutzen and Andreae, 1990). These pollutants alter the regional climate of downwind areas by altering ambient temperature, cloud properties, and precipitation efficiency (Jeong et al., 2008; Youn et al., 2011; Jeong et al., 2014). They also influence the air quality of downwind areas in urban, ocean, and Arctic regions through long-range atmospheric transport (Carvalho et al., 2011; Quennehe et al., 2012; Schreier et al., 2015).

During a severe forest fire episode in Moscow, Russia in August 2010, notably high concentrations of total carbon (mean of 202 μg m^{-3}) and levoglucosan (3.1 μg m^{-3}) were observed with an elevated organic carbon/elemental carbon (OC/EC) ratio of 27.4 (Popovicheva et al., 2014). Total carbon concentrations exceeded 10 times that during non-event periods in Moscow (Popovicheva et al., 2014). During severe forest fires in Siberia in May 2003, the surface PM_{10} (particulate matter with a diameter of ≤10 μm) and O_3 concentrations in downwind areas increased by 5–30 μg m^{-3} and 3–20 ppbv, respectively, and this had important implications for air quality over East Asia (Jeong et al., 2008).

Russia is covered by over 800 million hectares of forest, which is equal to 50 billion tons of growing carbon stock, where annually about 1% is damaged by fires (Bondur, 2010; Popovicheva et al., 2014). Russian boreal forests are subjected to frequent wildfires. Each year, 10,000–35,000 forest fires covering 5000–53,000 km^2 (including 4000–10,000 km^2 of high intensity, stand-replacing fires) are detected in actively

protected portions of Russian forests (Bartalev et al., 1977; Isaev et al., 2002; Mei et al., 2011). Approximately 12,000–34,000 wildfires occurred every year between 1974 and 1993 (Conard and Eduard, 1996), which makes Siberia a major boreal forest fire area in global terms.

Frequent forest fires over Siberia have an impact on downwind areas in Mongolia, China, Korea, and the Northwest Pacific through long-range atmospheric transport (Kajii et al., 2002; Kanaya et al., 2003; Lee et al., 2005; Jeong et al., 2008; Youn et al., 2011). In May 2003, intense forest fires occurred over Siberia (Lee et al., 2005; Jeong et al., 2008; Youn et al., 2011). Satellite observations clearly show the transport of smoke plumes emitted from Siberian forest fires through Mongolia and eastern China, south to the Korean Peninsula (Lee et al., 2005). Simulations by Youn et al. (2011) showed a significant surface cooling of –3.5 K over forested regions of Siberia. These simulations also showed that smoke aerosol affected large-scale circulation and resulted in an increase in average rainfall rates of 2.9 mm day^{-1} over the Northwest Pacific. Jeong et al. (2008) reported that smoke plumes from Siberian forest fires in May 2003 acted mainly as a cooling agent, resulting in a negative radiative forcing of –5.8 W m^{-2} at the surface over East Asia.

Severe wildfires occurred in the forested regions of Russia during summer 2014. The intensity of wildfires during this period was three times larger than in 2013. According to Russia's ITAR-TASS news agency, ~12,600 forest fires had burned over 1.8 million hectares as of 16 July 2014. During this time, the most forest fires occurred in the Irkutsk and Yakutsk areas of Siberia. Over 200 forest fires covering 92,000 hectares occurred in Siberian forested regions as of 16 July 2014 (http://tass.ru/en/russia/740878). MODIS satellite RGB images clearly show that these

89 smoke plumes lasted more than a week and were transported south to Mongolia,
90 northern China, and the Korean Peninsula.

91 In this study, we investigate the smoke plumes emitted from Siberian forest fires
92 during late July 2014 and their long-range atmospheric transport to the Korean
93 Peninsula. The transport mechanism of these plumes is investigated based on satellite
94 image analysis and satellite-based lidar observations. We also characterize the chemical
95 composition of these plumes over the Korean Peninsula. Chemical characteristics of
96 anthropogenic pollutants from East China transported to the Korean Peninsula in the
97 middle of July 2014 are also investigated and compared with those originating from
98 Siberian forest fires.

99

100 ## 2. Experimental Methods

101 ### 2.1 Atmospheric aerosol sampling and sample preparation

102 Table 1 summarizes the measurement parameters and conditions of this study. Daily
103 $PM_{2.5}$ (particulate matter with a diameter of $\leq$ 2.5 μm) sampling was carried out at a
104 regional air-quality monitoring station (36.19°N, 127.24°E) centrally located in Daejeon,
105 Korea, from 4 to 31 July 2014. The samples were collected on pre-baked quartz fiber
106 filters (47 mm diameter, Pall-Life Sciences, USA) using an aerosol sampler (PMS-103,
107 APM, Korea) at a flow rate of 16.7 L min^{-1} on the rooftop of a comprehensive
108 monitoring building (~15 m above the ground) of the National Institute of
109 Environmental Research in Korea. Before and after sampling, the filter samples were
110 wrapped with aluminum foil and stored in a freezer at –20 ℃. A total of 31 filter
111 samples were collected in this study, and additional field blank filters were collected
112 before and after the sampling period.

Ultrapure water used in this study was prepared using a Labpure S1 filter and an ultra-violet (UV) lamp (ELGA, PureLab Ultra, USA). Resistivity and total organic carbon (TOC) values of the ultrapure water were maintained at 18.2 MΩ cm^{-1} and 4 ppb, respectively. To measure carbohydrates and water-soluble ions, a quarter of each filter sample was extracted with 10 mL of ultrapure water under ultrasonication for 30 min, and then passed through a disk filter (0.45 mm, Millipore, Millex-GV, Germany). Water extracts were stored in a refrigerator at 4 ℃ before analysis.

2.2 Analysis of the chemical composition of fine particles

Mass concentrations of $PM_{2.5}$ were measured using a beta-attenuation technique (BAM 1020, Met One Instruments), with an hourly averaging time resolution. The manufacturer reported the detection limit and measurement error of the beta-attenuation technique as 3.6 μg m^{-3} and 8%, respectively. In addition to $PM_{2.5}$ mass concentrations, the daily-averaged chemical composition of $PM_{2.5}$ was characterized through filter sampling and laboratory analysis. Because the $PM_{2.5}$ chemical composition measurements were made on a daily basis, daily-averaged $PM_{2.5}$ mass and chemical compositions were used in this study.

2.2.1 Levoglcosan and mannosan analysis

Levoglucosan and mannosan were analyzed using an improved high-performance anion-exchange chromatography (HPAEC) method with pulsed amperometric detection (PAD) (Engling et al., 2006; Jung et al., 2014). The HPAEC-PAD system uses an ion chromatograph consisting of an electrochemical detector and gold electrode unit, along with an AS40 auto-sampler (Dionex ICS-15000, Thermo Fisher Scientific, USA).

Levoglucosan and mannosan were separated in a CarboPak MA1 analytical column (4 × 250 mm) using a sodium hydroxide solution as the eluent. The detection limits of levoglucosan and mannosan were 3.0 and 0.7 ng m^{-3}, respectively. The calculated values for analytical error, defined as the ratio of the standard deviation to the average value, obtained from triplicate analyses of filter samples, were 1.9% and 0.73% for levoglucosan and mannosan, respectively.

2.2.2 Water-soluble inorganic ion analysis

Water-soluble inorganic ions were analyzed using an ion chromatograph (Dionex ICS-15000, Thermo Fisher Scientific, USA). Nitrate (NO_3^-) and sulfate (SO_4^{2-}) were separated using an IonPAC AS15 column with a 20 mM potassium hydroxide (KOH) eluent at a flow rate of 0.5 mL min^{-1}. The detection limits of NO_3^- and SO_4^{2-}, which are defined as three times the standard deviation of field blanks, were 0.01 and 0.11 μg m^{-3}, respectively. The analytical errors associated with NO_3^- and SO_4^{2-} were 2.3% and 1.7%, respectively. Sodium (Na^+), ammonium (NH_4^+), potassium (K^+), calcium (Ca^{2+}), and magnesium (Mg^{2+}) were separated using an IonPac CS-12A column (4 × 250 mm) with a 38 mM methanesulfonic acid (MSA) eluent at a flow rate of 1.0 mL min^{-1}. The detection limits of NH_4^+ and K^+ were 0.03 and 0.006 μg m^{-3}, respectively. The analytical errors associated with NH_4^+ and K^+ were 1.4% and o.73%, respectively.

2.2.3 Organic carbon/elemental carbon analysis

Carbonaceous $PM_{2.5}$ was measured using a semi-continuous organic carbon/elemental carbon (OC/EC) analyzer (Model RT3140, Sunset Lab). The air samples were drawn through a $PM_{2.5}$ sharp-cut cyclone at 8 L min^{-1}. The sampled

aerosol was then passed through a multichannel parallel-plate denuder with a carbon-impregnated filter to remove semi-volatile organic vapors, and then collected on a quartz-fiber filter. The sampled aerosol was analyzed based on the thermal-optical transmittance (TOT) protocol for pyrolysis correction and the NIOSH (National Institute for Occupational Safety and Health) method 5040 temperature profile (Birch and Cary, 1996; Jung et al., 2010). External calibration was performed using known amounts of sucrose. The detection limit of both OC and EC is 0.5 μg C m^{-3} for a 1 hr time resolution, according to the manufacturer. The uncertainty of OC and EC measurements has been reported as 5% (Polidori et al., 2006).

2.3 Satellite aerosol optical depth and air mass backward trajectories

The NOAA/ARL HYSPLIT (HYbrid Single-Particle Lagrangian Trajectory) air mass backward trajectory analysis (Draxler and Rolph, 2015; Rolph, 2015) and Moderate Resolution Imaging Spectro-radiometer (MODIS) satellite image analysis were used to characterize potential source regions and the transport pathway of the haze plume. Air mass backward trajectories ending at the sampling site (36.19°N, 127.24°E) in Daejeon, Korea were computed for heights of 200, 500, and 1000 m above ground level (AGL) using the HYSPLIT model. All back-trajectories were calculated at 00:00 UTC and 12:00 UTC (09:00 LT and 21:00 LT, respectively), extending back 96 h with a 1 h time interval. The calculated air mass pathways indicate the general airflow pattern rather than the exact pathway of air masses, because the typical error in traveled distance is up to 20% for trajectories computed from analyzed wind fields (Stohl, 1998).

This study used aerosol optical depth (AOD) data retrieved using the NASA MODIS algorithm version V5.2, referred to as Collection 005 (C005) (Levy et al.,

185 2007a, b), which are part of the MODIS Terra/Aqua Level-2 gridded atmospheric data
186 product and are available on the MODIS web site (http://modis.gsfc.nasa.gov/). Cloud-
187 screened level 1.5 sun-photometer data at sites in Yakutsk (61.66 °N, 129.37 °E; 118 m
188 above sea level) and Ussuriysk (43.70°N, 132.16°E; 280 m above sea level) in Russia
189 were obtained from the AERONET site (http://aeronet.gsfc.nasa.gov). This study used
190 total column-integrated spectral AOD determined using the AERONET algorithm
191 (Dubovik and King, 2000).

192 CALIOP (Cloud-Aerosol Lidar with Orthogonal Polarization) is a space-based lidar
193 system onboard the Cloud Aerosol Lidar and Infrared Pathfinder Satellite Observations
194 (CALIPSO) satellite launched in 2006 (Winker et al., 2009). This study used version
195 2.30 data of total attenuated backscatter at 532 nm. Expedited CALIPSO images were
196 obtained from the CALIPSO website (http://www-
197 calipso.larc.nasa.gov/products/lidar/browse_images/show_calendar.php).

198

199 3. Results and Discussion

200 3.1 Overview of the chemical composition of $PM_{2.5}$

201 Figure 2 shows temporal variations in the chemical composition of $PM_{2.5}$ at the
202 Daejeon site throughout the entire measurement period. Daily average $PM_{2.5}$ mass
203 concentrations ranged from 8.0 to 65.1 μg m^{-3} with an average of 26.8 ± 15.4 μg m^{-3}.
204 Two peaks in $PM_{2.5}$ mass concentration were observed during 12–16 July (first episode)
205 and 27–28 July 2014 (second episode). $PM_{2.5}$ mass concentrations reached 65.1 and
206 56.2 μg m^{-3} during the first and second episodes, respectively. The temporal variations
207 in the sum of $PM_{2.5}$ chemical compositions show a similar pattern to that of total $PM_{2.5}$
208 mass (Fig. 2). The largest contribution to $PM_{2.5}$ mass during the measurement period

209 came from SO_4^{2-}, which had a mean of 8.8 ± 7.0 μg m^{-3}, followed by OC (4.3 ± 2.0 μg
210 m^{-3}), NH_4^+ (4.3 ± 3.3 μg m^{-3}), EC (1.1 ± 0.4 μg m^{-3}), and NO_3^- (1.0 ± 1.1 μg m^{-3}), with
211 minor contributions from Ca^{2+}, K^+, and Na^+.
212
213 3.2 Classification of haze episodes during summer 2014
214 3.2.1 Long-range transported smoke plumes from Siberian forest fires
215 The MODIS RGB images clearly show severe smoke plumes over the Siberian
216 forested region during late July 2014. Figure 3a shows a typical example from 25 July
217 2014 of satellite RGB images of the smoke plumes emitted from Siberian forest fires
218 and their atmospheric transport to the south. Fire events over the Siberian forested
219 region are indicated by red dots in Fig. 3a. It is clear that the smoke plumes originated
220 in Siberia and were transported south to the Korean Peninsula across Mongolia and
221 northeast China. HYSPLIT backward trajectory analyses (Fig. 3b) also indicate that
222 the air masses originated in the Siberian forested region and were transported to the
223 Korean Peninsula between 26 and 28 July 2014.
224 Figure 4 shows the horizontal distribution of AOD over East Asia from 23 to 28 July
225 2014. High values of AOD were observed over the Siberian forested region on 23 July,
226 when forest fires occurred. Peak values of AOD were then observed to shift southward
227 to northeast China and the Korean Peninsula from 23 to 28 July 2014 (Fig. 4). These
228 horizontal distributions of AOD also support the transport of smoke plumes emitted
229 from Siberian forest fires onto the Korean Peninsula during late July 2014.
230 Figure 5 shows temporal variations in AOD measured using a sun-photometer at the
231 Yakutsk and Ussuriysk sites. The Yakuksk site is located near the source of Siberian
232 forest fire emissions, whereas the Ussuriysk site is located just to the north of the

Korean Peninsula (Fig. 3). The measured AOD at the Yakutsk site started to increase from 23 July, and high AOD continued until 26 July 2014. The AOD dropped to <0.5 during 6:00−10:00 UTC, 25 July and increased again during 26 July. Because high AOD at the Yakutsk site was caused by transport of the Siberian smoke plume (Fig. 3), the sharp drop in AOD observed during 25 July can be explained by a change in wind direction at the Yakutsk site. The maximum AOD (~4) was observed at the Yakutsk site on 24 July 2014 during a Siberian forest fire event. High values for AOD were observed for 4 days at the Yakutsk site during the Siberian forest fire episode. Interestingly, a sharp increase in AOD was also observed at the Ussuriysk site on 24 July 2014. Spatial distributions of AOD from the MODIS satellite data (Fig. 4) clearly show that the Siberian smoke plumes extended over the Ussuriysk site during 24 July 2014. These results again suggest the transport of Siberian smoke plumes to the northern Korean Peninsula.

Figure 6 shows MODIS RGB images and vertical distributions of total attenuated backscatter at a wavelength of 532 nm measured by the CALIPSO satellite during 24, 25, and 27 July 2014. The left column in Fig. 6 shows MODIS RGB images taken during the Siberian smoke episode. These images show smoke plumes originating from the Siberian forest and being transported over northeastern China. The yellow lines over the images in the left column of Fig. 6 indicate the route of the CALIPSO satellite, and correspond to the x-axis of the backscatter plots shown in the right column of Fig. 6. In the total attenuated backscatter measurement plots (Fig. 6, right), red and yellow represent atmospheric aerosol particles and white represents clouds. Figure 6a and b clearly show that between 24 and 25 July 2014, a smoke layer existed approximately 3–5 km in height near the source region of the Siberian forest fires. As shown in Fig.

6c, the height of the smoke layer decreased to below 2 km on 27 July 2014 as it reached the Korean Peninsula.

The spatial distribution of AOD obtained from the MODIS and CALIPSO satellite observations, and the HYSPLIT air mass backward trajectory analysis indicate that smoke plumes originated from Siberian forest fires between 23 and 24 July 2014 and were transported over 3000 km south to the Korean Peninsula between 27 and 28 July 2014. Ground-based AOD measurements using a sun-photometer near the Siberian forest fire area and on the Korean Peninsula also support the transport of a smoke plume originating from Siberian forest fires onto the Korean Peninsula. Thus, the smoke episode observed between 27 and 28 July 2014 is hereafter referred to as the Siberian forest fire episode.

3.2.2 Long-range transported haze from Asian continental outflow

Besides the haze episode caused by the long-range transport of smoke emitted from Siberian forest fires during late July 2014, another haze episode was observed at the Daejeon site between 14 and 16 July 2014, as shown in Fig. 2. The MODIS RGB image from 14 July (Fig. 7) shows a severe haze plume originating from East China and extending to the Korean Peninsula across the Yellow Sea. HYSPLIT backward air mass trajectories also indicate the transport of air masses originating in East China to the Korean Peninsula over the Yellow Sea between 15 and 16 July 2014.

The region of East China extending from Beijing to Shanghai consists of heavily populated and industrialized cities (Chan and Yao, 2008). Large amounts of anthropogenic pollutants are emitted from this region (Li et al., in press). Figure 8 shows the horizontal distribution of MODIS AOD over East Asia from 13 to 16 July

2014. A trail of high AOD extending from East China to the Korean Peninsula over the Yellow Sea is evident, which suggests that the haze episode observed between 14 and 16 July 2014 was caused primarily by long-range transport of pollutants originating from East China. Thus, the haze episode observed between 14 and 16 July is hereafter referred to as the Chinese haze episode.

3.3 Chemical characterization of long-range transported haze plumes

3.3.1 Comparison of $PM_{2.5}$ chemical composition during haze episodes

Figure 9 shows temporal variations in $PM_{2.5}$ mass concentration and selected chemical components. During the Chinese haze episode, elevated concentrations of SO_4^{2-} (23.1 ± 2.1 μg m^{-3}) and K^+ (0.27 ± 0.08 μg m^{-3}) were observed, whereas elevated concentrations of levoglucosan (119.6 ± 6.0 ng m^{-3}), K^+ (0.33 ± 0.07 μg m^{-3}), and OC (10.8 ± 1.1 μg m^{-3}) were measured during the Siberian forest fire episode. As shown in Fig. 9, OC concentrations were relatively constant throughout the measurement period, except during the Siberian forest fire episode. However, several peaks in SO_4^{2-} concentration were observed, with the highest peak occurring during the Chinese haze episode.

It has been reported that biomass burning (including biofuel) contributed 14.1% of the total VOC emissions in China during 2012, whereas in Anhui province the contribution of biomass combustion to VOC emissions was 28.7% (Wu et al., 2016). Li et al. (2015) reported that biomass burning contributed 58% of OC in Nanjing, China during summer 2012, suggesting that biomass burning is the dominant source of OC in this region. Du et al. (2011) classified the haze events in Shanghai, China during summer 2009 into three categories: biomass-burning induced (high K^+, low SO_4^{2-} and

305 NO_3^-), complicated (high SO_4^{2-} and NO_3^-, good correlation between K^+ and SO_4^{2-} and
306 NO_3^-), and secondary (high SO_4^{2-} and NO_3^-, low K^+) pollution. Because Anhui,
307 Nanjing, and Shanghai are located near the source of the long-range transported
308 Chinese haze (Fig. 8), the chemical composition of pollution in those areas can be used
309 to understand the Chinese haze episode observed in this study. Temporal patterns in K^+
310 concentration are similar to those of SO_4^{2-}, and a sharp increase in SO_4^{2-} concentration
311 was observed during the Chinese haze episode (Fig. 9). This type of pollution episode
312 is similar to the 'complicated' pollution described by Du et al. (2011), and suggests
313 that the Chinese haze episode was caused mainly by secondary aerosol such as SO_4^{2-}
314 and NH_4^+, rather than by biomass burning emissions.

315 Figure 10 shows relative contributions to $PM_{2.5}$ mass during the Chinese haze and
316 Siberian forest fire episodes. Concentrations of organic aerosol (OM) were
317 reconstructed from measured OC concentrations by multiplying the OM/OC ratio of
318 1.8 that was measured using an aerosol mass spectrometer in Korea from spring to fall
319 2011 in the Asian continental outflow (Prof. T. Lee, pers. comm.). Huang et al. (2011)
320 reported a similar OM/OC ratio of 1.77 ± 0.08 measured at a downwind site of the
321 highly polluted Pearl River Delta cities in China during fall 2008. During the Chinese
322 haze episode, SO_4^{2-} was found to be the dominant species in $PM_{2.5}$ mass with an
323 average contribution of 44.2%, followed by OM (16.6%) and NH_4^+ (19.1%). This
324 result suggests that the Chinese haze episode can be attributed primarily to
325 anthropogenic pollutants (possibly emissions from industrial complexes and urban
326 cities in East China). However, during the Siberian forest fire episode, OM was the
327 dominant species in $PM_{2.5}$ mass with an average contribution of 38.6%, followed by
328 SO_4^{2-} (16.5%) and NH_4^+ (10.0%). The high concentration of OM indicates that the

329 Siberian forest fire episode originated primarily from biomass burning.

330

331 3.3.2 Comparison of biomass burning tracers during two haze episodes in the Daejeon
332 atmosphere

333 Levoglucosan and K^+ are widely used as indicators of biomass burning.
334 Levoglucosan is formed during pyrolysis of cellulose and hemicellulose, and is not
335 emitted from the burning of other materials, such as fossil fuels (Simoneit et al., 1999;
336 Caseiro et al., 2009; Elias et al., 2001). However, caution is required when using K^+ as a
337 biomass-burning tracer because K^+ can also be emitted from sea salt and soil (Pio et al.,
338 2008). The mass concentration of biomass burning tracers and their ratios during the
339 Siberian forest fire and Chinese haze episodes are summarized in Tables 2 and 3.

340 Significantly elevated concentrations of levoglucosan were observed during the
341 Siberian forest fire episode, compared with smaller increases observed during the
342 Chinese haze episode (Fig. 9). Concentrations of levoglucosan during the Siberian
343 forest fire episode were measured to be 119.6 ± 6.0 ng m^{-3}, approximately 6 times
344 higher than those during the Chinese haze episode (22.3 ± 11.8 ng m^{-3}), as listed in
345 Table 2. However, similar levels of K^+ were obtained during the Chinese haze (0.27 ±
346 0.08 μg m^{-3}) and Siberian forest fire (0.33 ± 0.07 μg m^{-3}) episodes. Thus, relatively
347 high levoglucosan/K^+ ratios were observed during the Siberian forest fire episode (0.37
348 ± 0.06) compared with those (0.08 ± 0.03) observed during the Chinese haze episode
349 (Table 3). However, the levoglucosan/mannosan ratios observed during the Siberian
350 forest fire episodes (3.43 ± 0.11) are similar to those observed during the Chinese haze
351 episodes (4.81 ± 0.41), as shown in Table 3.

352 OC concentrations increased as levoglucosan and K^+ concentrations increased

during the Siberian forest fire episode (Fig. 11a). Elevated OC/EC ratios were also observed during the Siberian forest fire episode (7.18 ± 0.2). Simultaneous increases in K^+, OC (Fig. 11b), and levoglucosan concentrations (Fig. 11c) during the Siberian forest fire episode suggest that the K^+ originated primarily from the smoke plume during the Siberian forest fire episode.

OC and levoglucosan concentrations observed during the Chinese haze episode are similar to those observed during the non-episode period, as shown in Fig. 11a. However, small increases in K^+ concentration were observed during the Chinese haze episode, as shown in Fig. 11b, resulting in relatively small levoglucosan/K+ ratios during the Chinese haze episode (0.08 ± 0.03) compared with those during the Siberian forest fire episode (0.37 ± 0.06). This difference in levoglucosan/K^+ ratios can be explained as follows. First, different types of biomass burning might have occurred during the Chinese haze episode compared with the Siberian forest fire episode. It can be postulated that biomass-burning emissions with relatively low OC/K^+ and levoglucosan/K^+ ratios might have contributed to observations made on the Korean Peninsula during the Chinese haze episode.

Second, K^+ measured during the Chinese haze episode may have originated from sources other than biomass burning. Because OC is predominantly emitted from biomass burning, biomass-burning particles have relatively high OC/EC ratios and are generally well correlated with biomass burning tracers (Cao et al., 2008; Cheng et al., 2008; Popovicheva et al., 2014). The lack of significant increases in OC/EC ratio (2.4 ± 0.4), and OC and levoglucosan concentrations during the Chinese haze episode compared with non-episode measurements suggests that the elevated K^+ concentrations observed during the Chinese haze episode might be due to emissions from other sources,

such as soil, sea salt, or industrial complexes. Chow et al. (2008) reported that 3.9%–12.5% of $PM_{2.5}$ consisted of K^+ in stack samples from cement kiln manufacturing processes. Positive correlations of K^+ with SO_4^{2-} and EC concentrations during the Chinese haze episode (Fig. 9) also suggest that there were additional emissions of K^+ from anthropogenic sources other than biomass burning.

Elevated concentrations of levoglucosan and OC, and relatively high OC/EC ratios (7.18 ± 0.2) suggest that the haze episode that occurred during late July 2014 was caused primarily by the long-range transport of smoke emitted from Siberian forest fires. However, significantly elevated SO_4^{2-} concentrations with relatively weak increases in OC and levoglucosan concentrations and lower OC/EC ratios indicate that the Chinese haze episode was caused primarily by anthropogenic pollutants emitted from industrial complexes and urban cities in East China, with relatively little contribution from biomass burning.

3.3.3 Tracking major sources of biomass burning during the Siberian forest fire episode

Levoglucosan/mannosan (Levo/Man) ratios and levoglucosan/K^+ (Levo/K^+) ratios observed during the Siberian forest fire episode are compared with those from previous chamber experiments and field studies in Fig. 12. Hardwood burning produces higher Levo/Man ratios with a mean value of 26 (range: 2.2–195) (Fine et al., 2001, 2002, 2004a, 2004b; Schauer et al., 2001; Engling et al., 2006; Schmidl et al., 2008a; Bari et al., 2009; Gonçalves et al., 2010), whereas softwood burning has lower Levo/Man ratios (mean: 4.3, range: 2.5–6.7) (Fine et al., 2001, 2002, 2004a, 2004b; Schauer et al., 2001; Hays et al., 2002; Engling et al., 2006; Iinuma et al., 2007; Schmidl et al., 2008a; Gonçalves et al., 2010). Grass (mean: 18, range: 9.2–39) and crop residue burnings

(mean: 29, range: 12–55) have relatively high Levo/Man ratios compared with leaf burning (mean: 5.6, range: 5.1–6.0) (Sheesley et al., 2003; Engling et al., 2006, 2009; Sullivan et al., 2008; Schmidl et al., 2008b; Oanh et al., 2011; Cheng et al., 2013). Levo/Man ratios (mean: 5.3) observed during the smoke episode in Moscow, Russia in summer 2010 are similar to those reported for softwood and leaf burning (Popovicheva et al., 2014).

Because levoglucosan and mannosan are emitted from similar burning processes, the Levo/Man ratio can be used to track the type of biomass burning. Levo/Man ratios observed during the Siberian forest fire episode are similar to those obtained from the softwood and leaf burning experiments, and the smoke episode in Moscow, Russia during summer 2010. However, Levo/Man ratios during the Siberian forest fire episode are much lower than those reported for hardwood, grass, and crop residue burning.

Hardwood and softwood burning yields relatively high Levo/K^+ ratios, with mean values of 26 and 46, and ranges of 2.2–195 and 4.6–261, respectively (Fine et al., 2001, 2002, 2004a, 2004b; Schauer et al., 2001; Hays et al., 2002; Engling et al., 2006; Iinuma et al., 2007; Schmidl et al., 2008a; Bari et al., 2009; Gonçalves et al., 2010). However, grass, crop residue, and leaf burning have relatively low Levo/K^+ ratios, with mean values of 3.3, 0.53, and 2.9, and ranges of 0.06–9.5, 0.1–1.2, and 2.4–3.4, respectively (Sheesley et al., 2003; Engling et al., 2006, 2009; Sullivan et al., 2008; Schmidl et al., 2008b; Oanh et al., 2011; Cheng et al., 2013). Levo/K^+ ratios (mean: 2.8) observed during the smoke episode in Moscow, Russia in summer 2010 are similar those reported for grass, crop residue, and leaf burning (Popovicheva et al., 2014).

Levo/K^+ ratios observed during the Siberian forest fire episode are close to those reported for grass, crop residue, and leaf burning, as well as to the ratios of the smoke

episode in Moscow, but much lower than those from hardwood and softwood burning (Fig. 12b). Levoglucosan can be removed through photo-oxidative decay during atmospheric transport (Hennigan et al., 2010), but K^+ is relatively stable in the atmosphere. Thus, Levo/K^+ ratios can decrease during long-range atmospheric transport. The Levo/K^+ ratios observed during the Siberian forest fire episode were lower than those during the smoke episode in Moscow, Russia in summer 2010, which can be explained by photochemical degradation of levoglucosan during long-range atmospheric transport.

Based on a comparison of biomass burning tracers from various sources (Fig. 12), it is suggested that smoke aerosol emitted during the Siberian forest fire episode originated mainly from the burning of forest leaves in Siberia prior to their long-range atmospheric transport. Smoke aerosol observed during the smoke episode in Moscow, Russia in summer 2010 have similar Levo/Man and Levo/K^+ ratios to those from leaf burning (Fig. 12). These observations suggest that smoke episodes in the Russian forest originate primarily from the burning of forest leaves.

4. Conclusion

This study investigated the long-range transport of smoke plumes emitted from Siberian forest fires during late July 2014. Smoke plumes emitted from Siberian forest fires are generally transported to the Northwest Pacific by prevailing westerlies. However, the haze plume that occurred during late July 2014 had a significant impact on the Korean Peninsula, which is located ~3000 km south of the Siberian forest. From the spatial distributions of AOD obtained from the MODIS satellite, CALIPSO satellite observations, and HYSPILT air mass backward trajectory analyses, it is evident that

smoke plumes originating from Siberian forest fires between 23 and 24 July 2014 were transported over 3000 km south to the Korean Peninsula between 27 and 28 July 2014. During this episode, elevated concentrations of levoglucosan (119.6 ± 6.0 ng m^{-3}) and K^+ (0.33 ± 0.07 μg m^{-3}), and high OC/EC ratios (7.18 ± 0.2) were observed at a measurement site in Daejeon, Korea. These results suggest that the haze episode that occurred during late July 2014 was caused mainly by the long-range transport of smoke plumes emitted from Siberian forest fires. The Siberian smoke episode is clearly distinguished from a haze episode caused by the long-range transport of anthropogenic pollutants emitted from East China, which was characterized by elevated SO_4^{2-} concentrations and weak increases in OC and levoglucosan concentrations.

Acknowledgements

This work was conducted as part of a co-research project between National Institute of Environmental Research (NIER) and the Korean Research Institute of Standards and Science (KRISS). This work was funded by the National Research Foundation under grant NRF-2015R1C1A1A02036580. We thank Dr. B. Holben and Dr. M. Panchenko for their efforts in establishing and maintaining the Yakutsk and Ussuriysk AERONET sites in Russia. The authors gratefully acknowledge the NOAA Air Resources Laboratory (ARL) for the provision of the HYSPLIT transport and dispersion model and the READY website (http://www.arl.noaa.gov/ready.html) used in this publication. The authors also thank NASA (USA) for making available the Collection 005 Level-2 MODIS data.

Reference

Bartalev, S. A., Korovin, G. N., and Shlepak, B. V.: Assessments of Forest Fire Recognition, Using the NOAA AVHRR Radiometers, in: Proceedings of International Forum on Problems in Science, Technology and Education, Vol. II, Moscow, 22–25, 1977.

Bari, M. A., Baumbach, G., Kuch, B., and Scheffknecht, G.: Wood smoke as a source of particle-phase organic compounds in residential areas, Atmos. Environ., 43, 4722–4732, 2009.

Birch, M. E., and Cary, R. A.: Elemental carbon-based method for monitoring occupational exposure to particulate diesel exhaust, Aerosol Sci. Tech., 25, 221–241, 1996.

Bondur, V. G.: Importance of aerospace remote sensing approach to the monitoring of nature fire in Russia, International Forest Fire News (IFFN), (40), 43–57, 2010.

Cao, G., Zhang, X., Gong, S., and Zheng, F.: Investigation on emission factors of particulate matter and gaseous pollutants from crop residue burning, J. Environ. Sci., 20, 50–55, 2008.

Carvalho, A., Monteiro, A., Flannigan, M., Solman, S., Miranda, A. I., and Borrego, C.: Forest fires in a changing climate and their impacts on air quality, Atmos. Environ., 45, 5545–5553, 2011.

Caseiro, A., Bauer, H., Schmidl, C., Pio, C. A., and Puxbaum, H.: Wood burning impact on PM_{10} in three Austrian regions, Atmospheric Environment, 43, 2186–2195, 2009.

Chan, C. K., and Yao, X.: Air pollution in mega cities in China, Atmos. Environ., 42, 1–42, 2008.

Cheng, M. T., Horng, C. L., Su, Y. R., Lin, L. K., Lin, Y. C., and Chou, C. K.: Particulate matter characteristics during agricultural waste burning in Taichung City, Taiwan, J. Hazard. Mater., 165, 187–192, 2008.

Cheng, Y., Engling, G., He, K. B., Duan, F. K., Ma, Y. L., Du, Z. Y., Liu, J. M., Zheng, M., and Weber., R. J.: Biomass burning contribution to Beijing aerosol, Atmos. Chem. Phys., 13, 7765–7781, 2013.

Chow, J. C., Watson, J. G., Kuhns, H., Etyemezian, V., Lowenthal, D. H., Crow, D.,

Kohl, S. D., Engelbrecht, J. P., and Green, M. C.: Source profiles for industrial, mobile, and area sources in the Big Bend Regional Aerosol Visibility and Observational study, Chemosphere, 54, 185–208, 2004.

Conard, S. G., and Ivanova, G. A.: A Differential Approach to Numerical Assessment of Forest Fire Carbon Emissions, Lesovedenie (Forestry), 3, 28–35, 1988.

Crutzen, P., Heidt, L., Krasnec, J., Pollock, W., and Seiler, W.: Biomass burning as a source of atmospheric gases CO, H_2, N_2O, NO, CH_3Cl and COS, Nature, 282 (5736), 253–256, 1979.

Du, H., Kong, L, Cheng, T., Chen, J., Du, J., Li, L., Xia, X., Leng, C., and Huang, G.: Insights into summertime haze pollution events over Shanghai based on online water-soluble ionic composition of aerosols, Atmos. Environ., 45, 5131–5137, 2011.

Elias, V. O., Simoneit, B. R. T., Cordeiro, R. C., and Turcq,B.: Evaluating levoglucosan as an indicator of biomass burning in Carajás, Amazônia: a comparison to the charcoal record, Geochim. Cosmochim. Acta, 65, 267–272, 2001.

Engling, G., Carrico, C.M., Kreidenweis, S. M., Collett Jr, J. L., Day, D. E., Malm, W. C., Lincoln, L., Hao, W. M., Iinuma, Y., and Herrmann, H.: Determination of levoglucosan in biomass combustion aerosol by high-performance anion-exchange chromatography with pulsed amperometric detection, Atmos. Environ., 40, S299–S311, 2006.

Engling, G., Lee, J. J., Tsai, Y. W., Lung, S. C. C., Chou, C. C. K., and Chan, C. Y.: Size-resolved anhydrosugar composition in smoke aerosol from controlled field burning of rice straw, Aerosol Sci. Tech., 43, 662–672, 2009.

Fine, P. M., Cass, G. R., and Simoneit, B. R. T.: Chemical characterization of fine particle emissions from fireplace combustion of woods grown in the northeastern United States, Environ. Sci. Tech., 35, 2665–2675, 2001.

Fine, P. M., Cass, G. R., and Simoneit, B. R. T.: Chemical characterization of fine particle emissions from the fireplace combustion of woods grown in the southern United States, Environ. Sci. Tech., 36, 1442–1451, 2002.

Fine, P. M., Cass, G. R., and Simoneit, B. R. T.: Chemical characterization of fine particle emissions from the fireplace combustion of wood types grown in the midwestern and western United States, Environ. Eng. Sci., 21, 387–409, 2004a.

Fine, P. M., Cass G. R., and Simoneit, B. R. T.: Chemical characterization of fine

particle emissions from the wood stove combustion of prevalent United States tree species, Environ. Eng. Sci., 21, 705–721, 2004b.

Gonçalves, C., Alves, C., Evtyugina, M., Mirante, F., Pio, C., Caseiro, A., Schmidl, C., Bauer, H., and Carvalho, F.: Characterisation of PM_{10} emissions from wood stove combustion of common woods grown in Portugal, Atmos. Environ., 44, 4474–4480, 2010.

Hays, M. D., Geron, C. D., Linna, K. J., Smith, N. D., and Schauer, J. J.: Speciation of gas-phase and fine particle emissions from burning of foliar fuels, Environ. Sci. Tech., 36, 2281–2295, 2002.

Hennigan, C. J., Sullivan, A. P., Collett Jr, J. L., and Robinson, A. L.: Levoglucosan stability in biomass burning particles exposed to hydroxyl radicals, Geophys. Res. Lett., 37, doi:10.1029/2010GL043088, 2010.

Huang, X. F., He, L., Hu, M., Cangaratna, M. R., Kroll, J. H., Ng, N. L., Zhang, Y. H., Lin, Y., Xue, L., Sun, T. L., Liu, X. G., Shao, M., Jayne, J. T., and Worsnop, D. R.: Characterization of submicron aerosols at a rural site in Pearl River Delta of China using an Aerodyne High-Resolution Aerosol Mass Spectrometer, Atmos. Chem. Phys., 11, 1865–1877, 2011.

Iinuma, Y., Brüggemann, E., Gnauk, T., Müller, K., Andreae, M. O., Helas, G., Parmar, R., and Herrmann, H.: Source characterization of biomass burning particles: The combustion of selected European conifers, African hardwood, savanna grass, and German and Indonesian peat, J. Geophys. Res., 112, D08209, doi:10.1029/2006JD007120, 2007.

Isaev, A. S., Korovin, G. N., Bartalev, S. A., Ershov, D. V., Janetos, A., Kasischke, E. S., Shugart, H. H., French, N. H. F., Orlick, B. E., and Murphy, T. L.: Using Remote Sensing to Assess Russian Forest Fire Carbon Emissions, Climatic Change, 55, 235–249, 2002.

Jeong, H., Chung, C. E., van Noije, T., and Takemura, T.: Relationship between fine-mode AOD and precipitation on seasonal and interannual time scales, Tellus Ser. B, 66, 23037, doi:10.3402/tellusb.v66.23037, 2014.

Jeong, J. I., Park, R. J., and Youn, D.: Effects of Siberian forest fires on air quality in East Asia during May 2003 and its climate implication, Atmos. Environ., 42, 8910–8922. doi:10.1016/j.atmosenv.2008.08.037, 2008.

Kajii, Y., Kato, S., Streets, D. G., Tsai, N. Y., Shvidenko, A., Nilsson, S., Minko, N. P., Abushenko, N., Altyntsev, D., and Khodzer, T. V.: Boreal forest fires in Siberia in 1998: estimation of area and emissions of pollutants by AVHRR satellite data, J. Geophys. Res., 107 (D24), 4745, 2002.

Kanaya, Y., Kajii, Y., and Akimoto, H.: Solar actinic flux and photolysis frequency determinations by radiometers and a radiative transfer model at Rishiri Island: comparisons, cloud effects, and detection of an aerosol plume from Russian forest fires, Atmos. Environ., 37 (18), 2463–2475, 2003.

Lee, K. H., Kim, J. E., Kim, Y. J., Kim, J., and Von Hoyningen-Huene, W.: Impact of the smoke aerosol from Russian forest fires on the atmospheric environment over Korea during May 2003, Atmos. Environ., 39, 85–99, 2005.

Li, B., Zhang, J., Zhao, Y., Yuan, S., Zhao, Q., Shen, G., and Wu, H.: Seasonal variation of urban carbonaceous aerosols in a typical city Nanjing in Yangtze River Delta, China, Atmos. Environ., 106, 223–231, 2015.

Li, L., An, J. Y., Zhou, M., Yan, R. S., Huang, C., Lu, Q., Lin, L., Wang, Y. J., Tao, S. K., Qiao, L. P., Zhu, S. H., and Chen, C. H.: Source apportionment of fine particles and its chemical components over the Yangtze River Delta, China during a heavy haze pollution episode, Atmos. Environ., http://dx.doi.org/10.1016/j.atmosenv.2015.06.051, 2015(in press).

Mei, L., Xue, Y., de Leeuw, G., Guang, J., Wang, Y., Li, Y., Xu, H., Yang, L., Hou, T., He, X., Wu, C., Dong, J., and Chen, Z.: Integration of remote sensing data and surface observations to estimate the impact of the Russian wildfires over Europe and Asia during August 2010, Biogeosciences, 8, 3771–3791, 2011.

Oanh, N. T. K., Ly, B. T., Tipayarom, D., Manandhar, B. R., Prapat, P., Simpson, C. D., and Liu, L. J. S.: Characterization of particulate matter emission from open burning of rice straw, Atmos. Environ., 45, 493–502, 2011.

Pio, C. A., Legrand, M., Alves, C. A., Oliveira, T., Afonso, J., Caseiro, A., Puxbaum, H., Sanchez-Ochoa, A., and Gelencsér, A.: Chemical composition of atmospheric aerosols during the 2003 summer intense forest fire period, Atmos. Environ., 42, 7530–7543, 2008.

Popovicheva, O., Kistler, M., Kireeva, E., Persiantseva, N., Timofeev, M., Kopeikin, V., and Kasper-Giebl, A.: Physicochemical characterization of smoke aerosol during

large-scale wildfires: Extreme event of August 2010 in Moscow, Atmos. Environ., 96, 405–414, 2014.

Quennehen, B., Schwarzenboeck, A., Matsuki, A., Burkhart, J. F., Stohl, A., Ancellet, G., and Law, K. S.: Anthropogenic and forest fire pollution aerosol transported to the Arctic: observations from the POLARCAT-France spring campaign, Atmos. Chem. Phys., 12, 6437–6454, 2012.

Schauer, J. J., Kleeman, M. J., Cass, G. R., and Simoneit, B. R. T.: Measurement of emissions from air pollution sources. 3. C1-C29 organic compounds from fireplace combustion of wood, Environ. Sci. Tech., 35, 1716–1728, 2001.

Schmidl, C., Marr, I. L., Caseiro, A., Kotianová, P., Berner, A., Bauer, H., Kasper-Giebl, A., and Puxbaum, H.: Chemical characterisation of fine particle emissions from wood stove combustion of common woods growing in mid-European Alpine regions, Atmos. Environ., 42, 126–141, 2008a.

Schmidl, C., Bauer, H., Dattler, A., Hitzenberger, R., Weissenboeck, G., Marr, I. L., and Puxbaum, H.: Chemical characterisation of particle emissions from burning leaves, Atmos. Environ., 42, 9070–9079, 2008b.

Schreier, S. F., Richter, A., Schepaschenko, D., Shvidenko, A., Hilboll, A., and Burrows, J.P.: Differences in satellite-derived NO_x emission factors between Eurasian and North American boreal forest fires, Atmos. Environ., 121, 55–65, 2015.

Sheesley, R. J., Schauer, J. J., Chowdhury, Z., Cass, G. R., and Simoneit, B. R. T.: Characterization of organic aerosols emitted from the combustion of biomass indigenous to South Asia, J. Geophys. Res., 108, 4285, doi:10.1029/2002JD002981, 2003.

Simoneit, B. R. T., Schauer, J. J., Nolte, C. G., Oros, D. R., Elias, V. O., Fraser, M. P., Rogge, W. F., and Cass, G. R.: Levoglucosan, a tracer for cellulose in biomass burning and atmospheric particles, Atmos. Environ., 33, 173–182, 1999.

Sullivan, A. P., Holden, A. S., Patterson, L. A., McMeeking, G. R., Kreidenweis, S. M., Malm, W. C., Hao, W. M., Wold, C. E., and Collett Jr., J. L.: A method for smoke marker measurements and its potential application for determining the contribution of biomass burning from wildfires and prescribed fires to ambient $PM_{2.5}$ organic carbon, J. Geophys. Res., 113, D22302, doi:10.1029/2008JD010216, 2008.

Wu, R., Bo, Y., Li, J., Li, L., Li, Y., and Xie, S.: Method to establish the emission

632 inventory of anthropogenic volatile organic compounds in China and its application
633 in the period 2008-2012, Atmos. Environ., 127, 244–254, 2016.
634 Youn, D., Park, R. J., Jeong, J. I., Moon, B. K., Yeh, S. W., Kim, Y. H., Woo, J. H., Im,
635 E. G., Jeong, J. H., Lee, S. J., and Song, C. K.: Impacts of aerosols on regional
636 meteorology due to Siberian forest fires in May 2003, Atmos. Environ., 45, 1407–
637 1412, 2011.

Table 1. Measurement parameters and conditions of the present study.

Measurement parameters	Site	Sampling method	Measurement method	Data frequency
$PM_{2.5}$ mass	Daejeon, Korea	Online measurement	Beta-attenuation monitor	1 h
Levoglucosan, Mannosan	Daejeon, Korea	$PM_{2.5}$ filter sampling	High-performance anion-exchange chromatography	1 day
Water-soluble ions (NO_3^-, SO_4^{2-}, etc)	Daejeon, Korea	$PM_{2.5}$ filter sampling	Ion chromatography	1 day
Organic carbon (OC), elemental carbon (EC)	Daejeon, Korea	Online measurement	Semi-continuous OC/EC analyzer	1 h
Aerosol optical depth (AOD)	Yakutsk and Ussuriysk, Russia	Online measurement	Sunphotometer	~15 min

Table 2. Summary of fine particle ($PM_{2.5}$) mass, and organic and inorganic chemical composition of $PM_{2.5}$ particles during the Chinese haze and Siberian forest fire episodes measured at Daejeon, Korea during summer 2014.

Components	Unit	[1)]Chinese Haze	[2)]Siberian Forest Fire
		Range (Average ± 1σ)	
$PM_{2.5}$ mass	($\mu g\ m^{-3}$)	44.5–65.1 (52.3 ± 11.1)	44.3–56.2 (50.2 ± 8.4)
SO_4^{2-}		20.9–25.1 (23.1 ± 2.1)	7.4–9.2 (8.3 ± 1.3)
NO_3^-		0.9–5.0 (2.8 ± 2.1)	1.1–1.7 (1.4 ± 0.4)
NH_4^+		6.1–12.7 (10.0 ± 3.5)	4.6–5.4 (5.0 ± 0.6)
OC		3.6–5.7 (4.8 ± 1.1)	10.0–11.6 (10.8 ± 1.1)
EC		1.9–2.2 (2.0 ± 0.2)	1.4–1.6 (1.5 ± 0.2)
K^+		0.17–0.33 (0.27 ± 0.08)	0.28–0.38 (0.33 ± 0.07)
OC/EC ratio	———	1.93–2.64 (2.4 ± 0.41)	7.04–7.32 (7.18 ± 0.19)
Levoglucosan	($ng\ m^{-3}$)	13.4–35.7 (22.3 ± 11.8)	115.4–123.9 (119.6 ± 6.0)
Mannosan		3.0–6.8 (4.5 ± 2.0)	32.9–37.0 (34.9 ± 2.9)

[1)]Chinese haze: 14–16 July 2014

[2)]Siberian forest fire: 27–28 July 2014

Table 3. Summary of ratios of biomass burning tracers during the Chinese haze and Siberian forest fire episodes, as measured at Daejeon, Korea in summer 2014.

Components	Chinese Haze	Siberian Forest Fire
	Range (Average ± 1σ)	
Levoglucosan/Mannosan ratio	4.41–5.22 (4.81 ± 0.41)	3.35–3.51 (3.43 ± 0.11)
Levoglucosan/K^+ ratio	0.05–0.11 (0.08 ± 0.03)	0.33–0.41 (0.37 ± 0.06)

Figure captions

Fig. 1. Map of the measurement site (36.19°N, 127.24°E) in Daejeon, Korea (base map from Google Maps). The Siberian forest is located ~3000 km north of the Korean Peninsula.

Fig. 2. Temporal variations in the chemical components of fine particulate matter ($PM_{2.5}$) at the Daejeon site during July 2014.

Fig. 3. (a) MODIS RGB image on 25 July 2014 and (b) air mass backward trajectories between 26 and 28 July 2014 when smoke plumes originating from Siberian forest fires had an impact on the Korean Peninsula. Red, blue, and green in (b) represent air mass backward trajectories arriving at 200 m, 500 m, and 1000 m heights, respectively. The Yakutsk site (61.66°N, 129.37°E) and Ussuriysk site (43.70°N, 132.16°E) in (b) are AERONET sites in Russia.

Fig. 4. MODIS AOD over East Asia from 23 to 28 July 2014.

Fig. 5. Temporal variations in AOD measured by a sun-photometer at the Yakutsk and Ussuriysk sites in Russia during July 2014.

Fig. 6. MODIS RGB images and vertical profiles of total attenuated backscatter at 532 nm measured by the CALIPSO satellite during (a) 24, (b) 25, and (c) 27 July 2014. Yellow lines in the MODIS RGB images indicate the route of the CALIPSO satellite, and correspond to the x-axis in the vertical profiles of total attenuated backscatter.

Fig. 7. (a) MODIS RGB image on 14 July 2014 and (b) air mass backward trajectories between 15 and 16 July 2014 when haze plumes originating from East China had an impact on the Korean Peninsula.

Fig. 8. MODIS AOD over East Asia between 13 and 15 July 2014.

Fig. 9. Temporal variations in $PM_{2.5}$ mass, K^+, levoglucosan, OC, EC, and SO_4^{2-} concentrations at the Daejeon site over the entire measurement period.

Fig. 10. Average relative contributions to $PM_{2.5}$ mass during the (a) Chinese haze and (b) Siberian forest fire episodes.

Fig. 11. Scatter plots of OC versus (a) levoglucosan and (b) K^+, and levoglucosan versus (c) K^+ and (d) mannosan between 4 and 31 July 2014. Filled black and red diamonds represent the Chinese haze and Siberian forest fire episodes, respectively. Open black circles represent the remaining sampling days in July 2014.

Fig. 12. (a) Levoglucosan to mannosan ratios and (b) levoglucosan to K^+ ratios obtained from previous chamber studies, extreme smoke episodes in Moscow, Russia in summer 2010, and the Siberian forest fire episode. **Hardwoods**: Fine et al. (2001, 2002, 2004a, 2004b), Schauer et al. (2001), Engling et al. (2006), Schmidl et al. (2008a), Goncalves et al. (2010), Bari et al. (2009); **Softwoods**: Fine et al. (2001, 2002, 2004a, 2004b), Schauer et al. (2001), Engling et al. (2006), Hay et al. (2002), Schmidl et al. (2008a), Goncalves et al. (2010), Iinuma et al. (2007), Cheng et al. (2013); **Grass**: Sullivan et al. (2008); **Crop residue**: Sullivan et al., (2008), Oanh et al. (2011), Sheesley et al. (2003), Engling et al. (2009), Cheng et al. (2013); **Leaf**: Schmidl et al. (2008b); **Moscow smoke:** Popovicheva et al. (2014); **LRT Siberia FF**: This study.

Figure 1

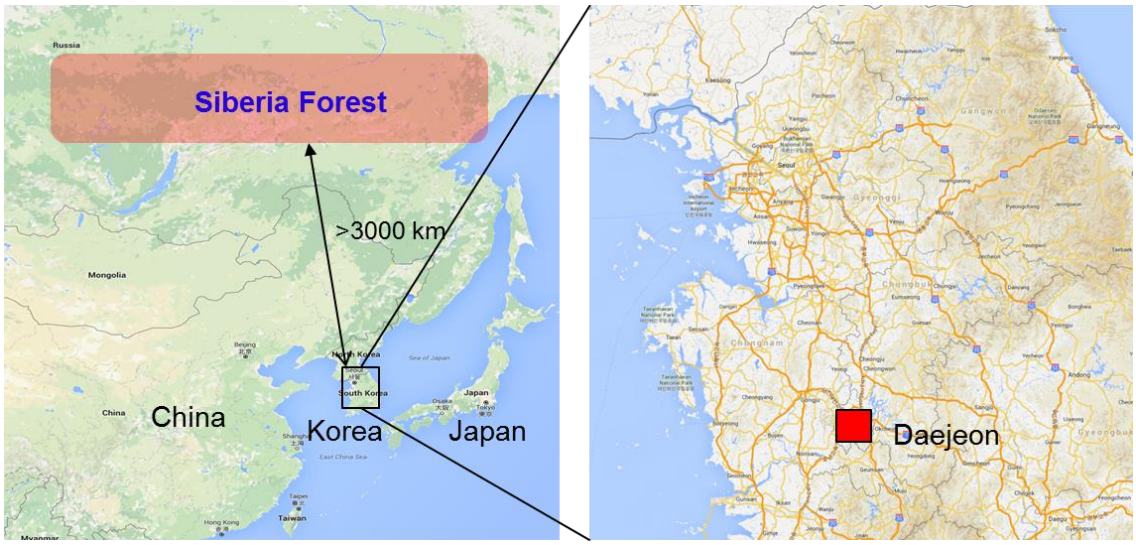

Figure 2

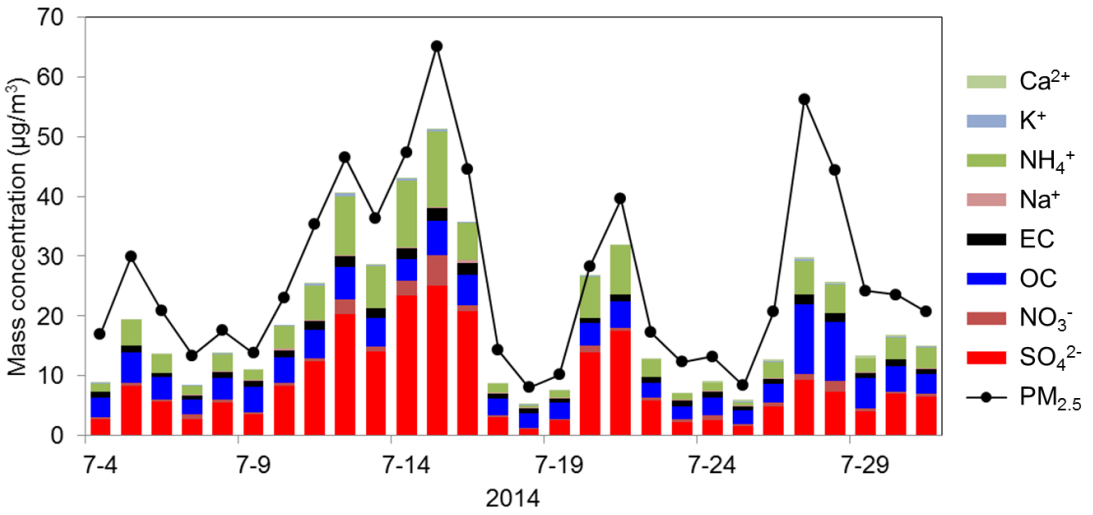
70
60
50
40
30
20
10
0
Mass concentration (μg/m3)
7-4
7-9
7-14
7-19
7-24
7-29
2014
Ca2+
K+
NH4+
Na+
EC
OC
NO3-
SO42-
PM2.5

Figure 3

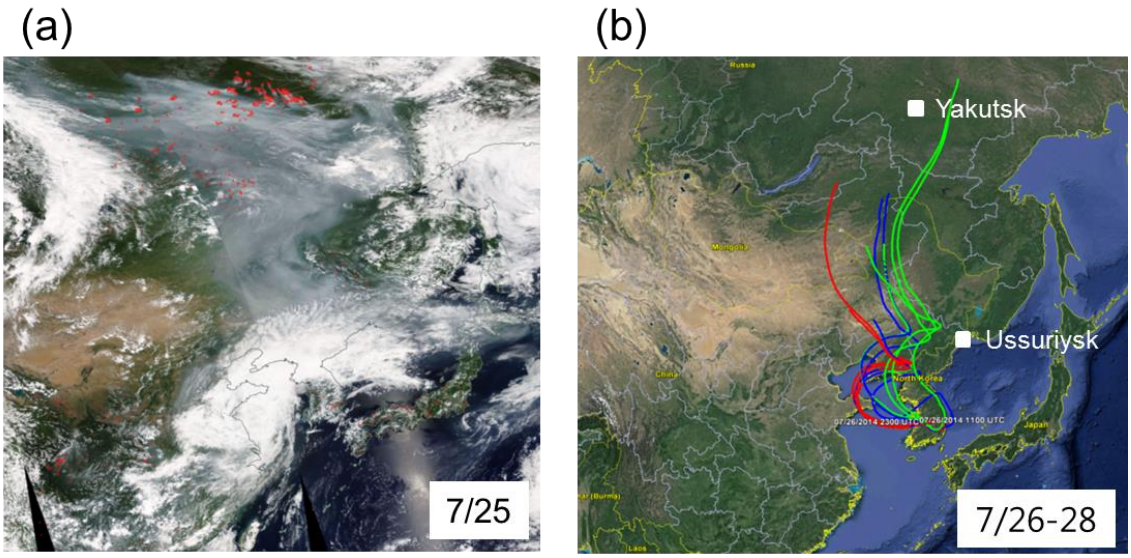

Figure 4

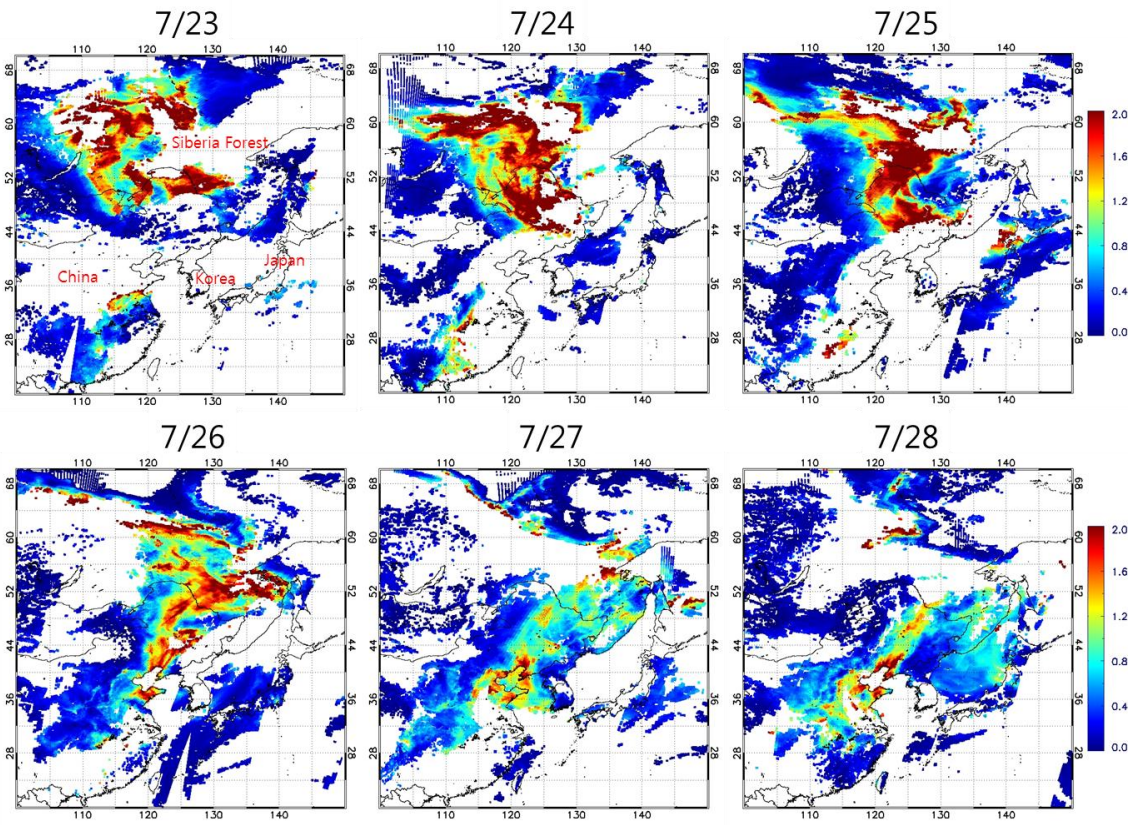
7/23
7/24
7/25
7/26
7/27
7/28
Siberia Forest
China
Korea
Japan
110
120
130
140
68
60
52
44
36
28
2.0
1.6
1.2
0.8
0.4
0.0

Figure 5

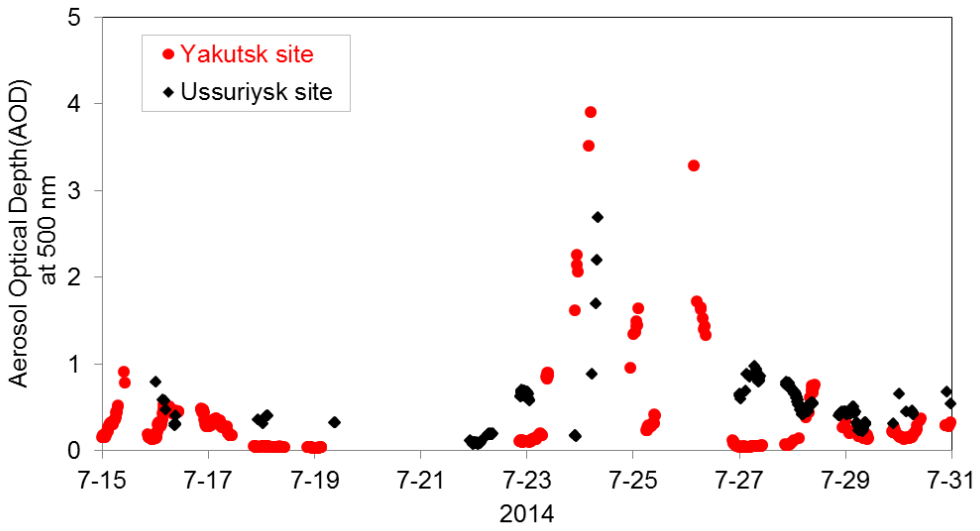
Yakutsk site
Ussuriysk site
Aerosol Optical Depth(AOD) at 500 nm
0
1
2
3
4
5
7-15
7-17
7-19
7-21
7-23
7-25
7-27
7-29
7-31
2014

Figure 6

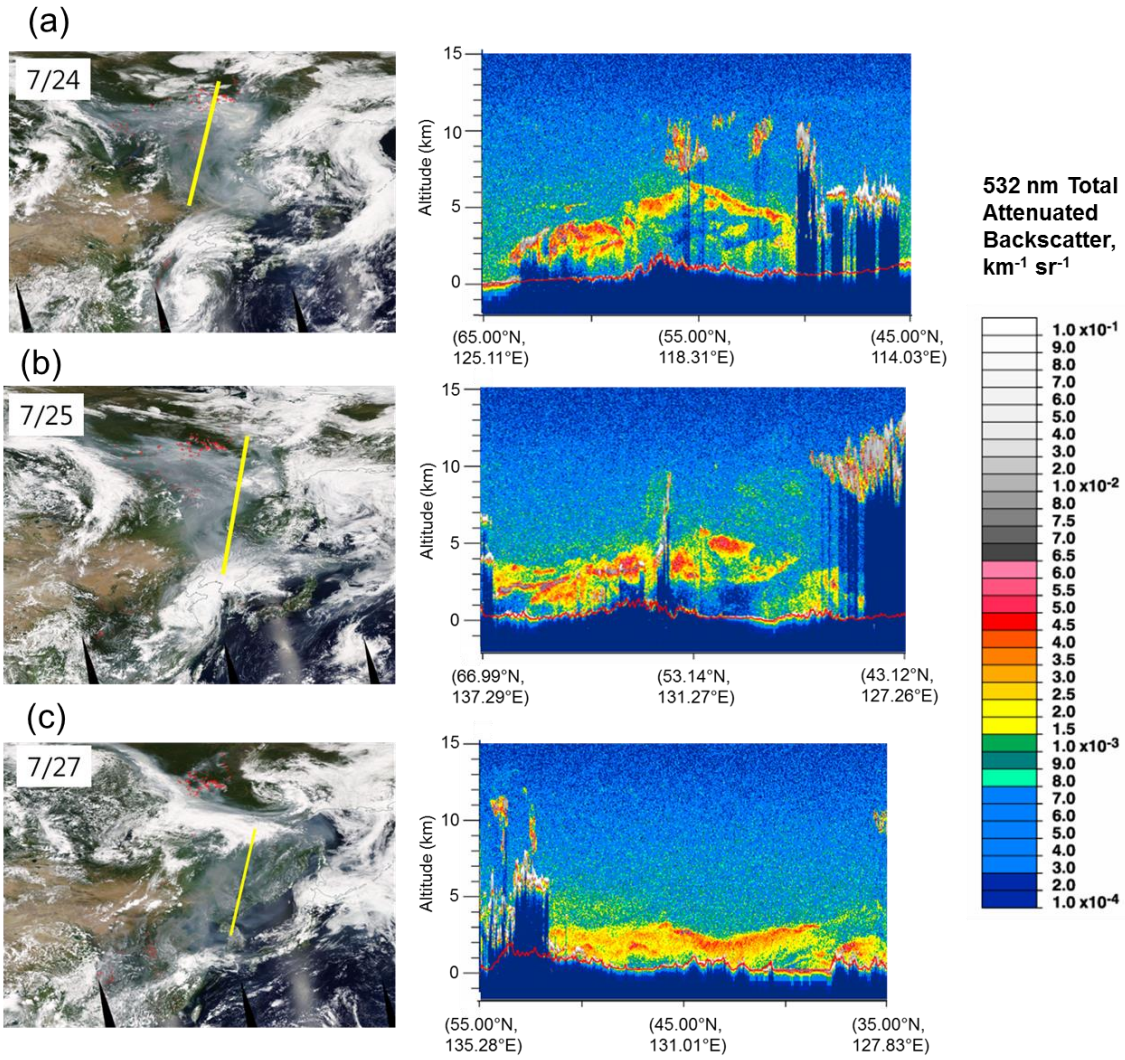
(a)
7/24
(b)
7/25
(c)
7/27
Altitude (km)
15
10
5
0
(65.00°N, 125.11°E)
(55.00°N, 118.31°E)
(45.00°N, 114.03°E)
(66.99°N, 137.29°E)
(53.14°N, 131.27°E)
(43.12°N, 127.26°E)
(55.00°N, 135.28°E)
(45.00°N, 131.01°E)
(35.00°N, 127.83°E)
532 nm Total Attenuated Backscatter, km-1 sr-1
1.0 x10-1
9.0
8.0
7.0
6.0
5.0
4.0
3.0
2.0
1.0 x10-2
8.0
7.5
7.0
6.5
6.0
5.5
5.0
4.5
4.0
3.5
3.0
2.5
2.0
1.5
1.0 x10-3
9.0
8.0
7.0
6.0
5.0
4.0
3.0
2.0
1.0 x10-4

Figure 7

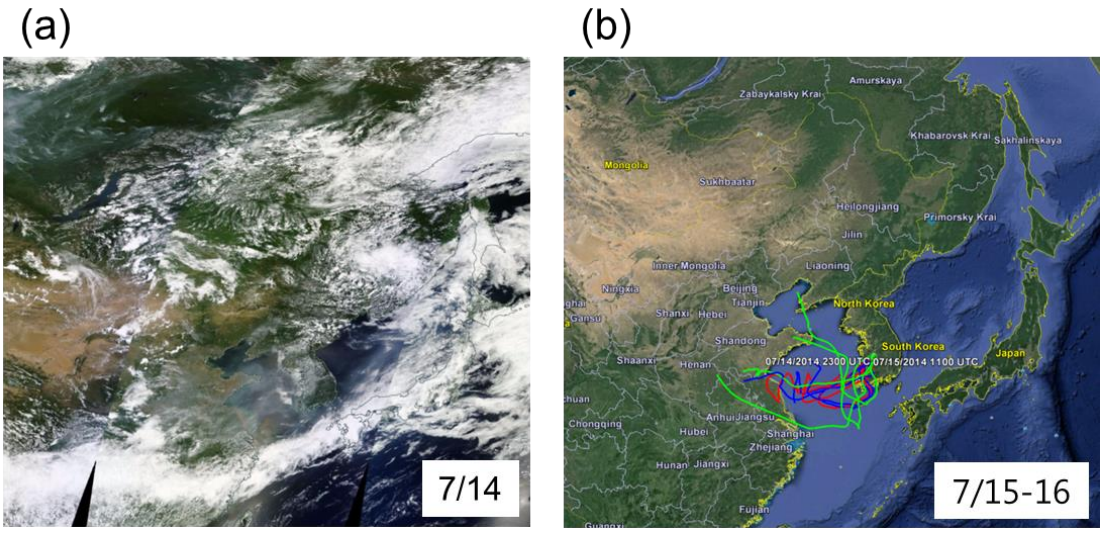
(a)
7/14
(b)
Amurskaya
Zabaykalsky Krai
Khabarovsk Krai
Sakhalinskaya
Mongolia
Sukhbaatar
Heilongjiang
Primorsky Krai
Jilin
Inner Mongolia
Liaoning
Ningxia
Beijing
Tianjin
North Korea
Shanxi
Hebei
Shandong
South Korea
Japan
Shaanxi
Henan
07/14/2014 2300 UTC
07/15/2014 1100 UTC
Chongqing
Anhui
Jiangsu
Hubei
Shanghai
Zhejiang
Hunan
Jiangxi
Fujian
7/15-16

Figure 8

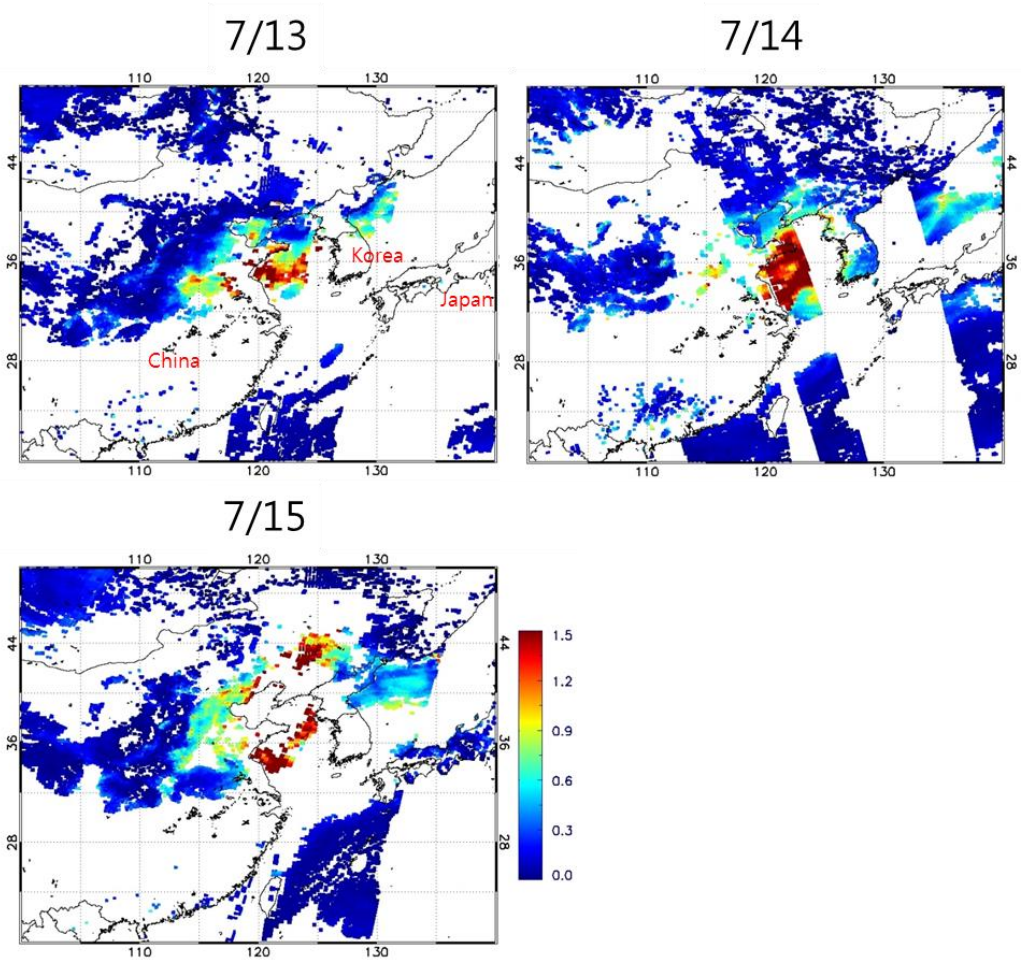
7/13
7/14
7/15
Korea
Japan
China
110
120
130
44
36
28
1.5
1.2
0.9
0.6
0.3
0.0

Figure 9

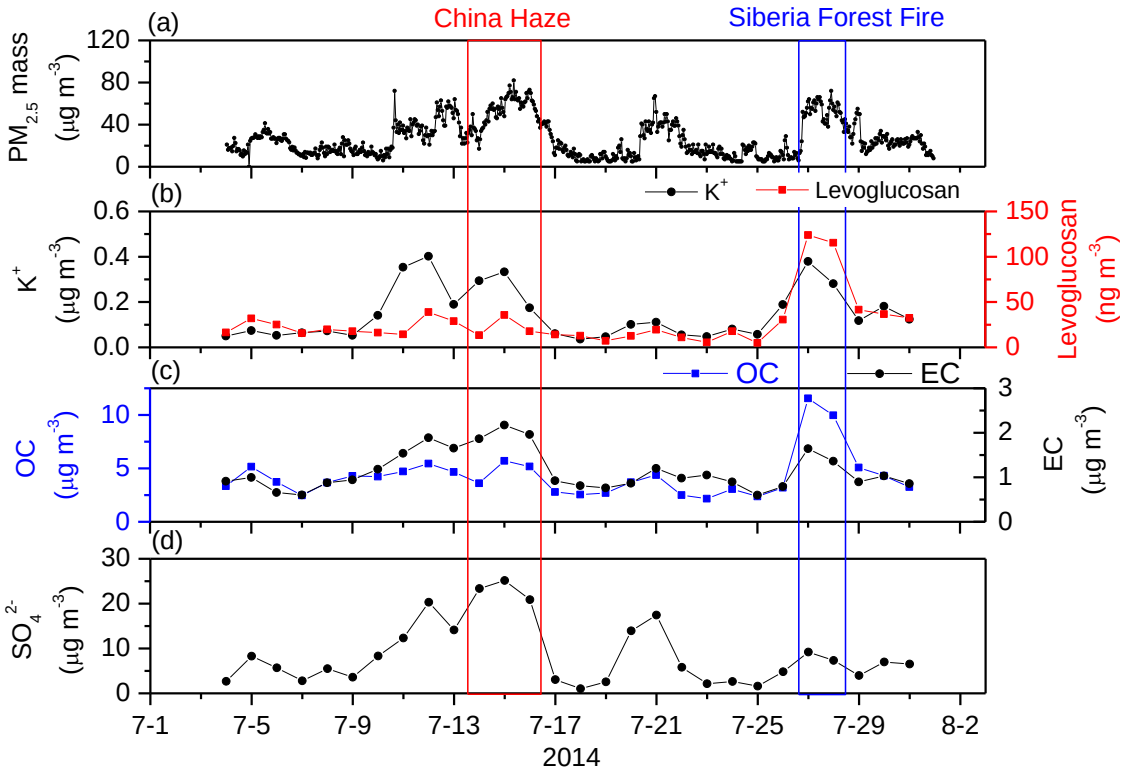
China Haze
Siberia Forest Fire
(a)
PM2.5 mass (μg m-3)
120
80
40
0
(b)
K+
Levoglucosan
K+ (μg m-3)
0.6
0.4
0.2
0.0
150
100
50
0
Levoglucosan (ng m-3)
(c)
OC
EC
OC (μg m-3)
10
5
0
3
2
1
0
EC (μg m-3)
(d)
SO4 2- (μg m-3)
30
20
10
0
7-1
7-5
7-9
7-13
7-17
7-21
7-25
7-29
8-2
2014

Figure 10

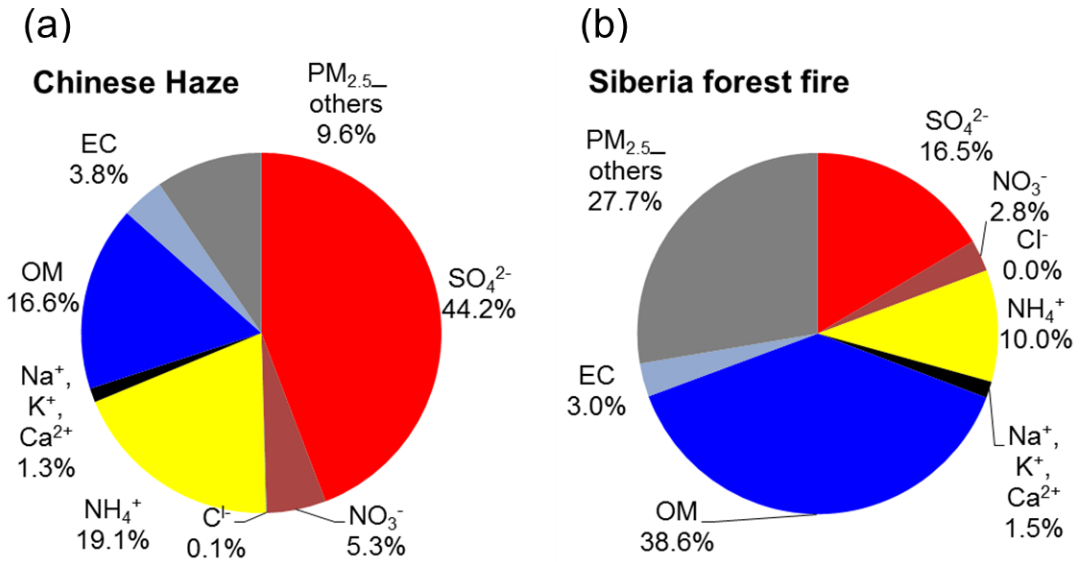
(a)
Chinese Haze
PM2.5 others 9.6%
EC 3.8%
OM 16.6%
Na+, K+, Ca2+ 1.3%
NH4+ 19.1%
Cl- 0.1%
NO3- 5.3%
SO42- 44.2%
(b)
Siberia forest fire
PM2.5 others 27.7%
SO42- 16.5%
NO3- 2.8%
Cl- 0.0%
NH4+ 10.0%
EC 3.0%
Na+, K+, Ca2+ 1.5%
OM 38.6%

Figure 11

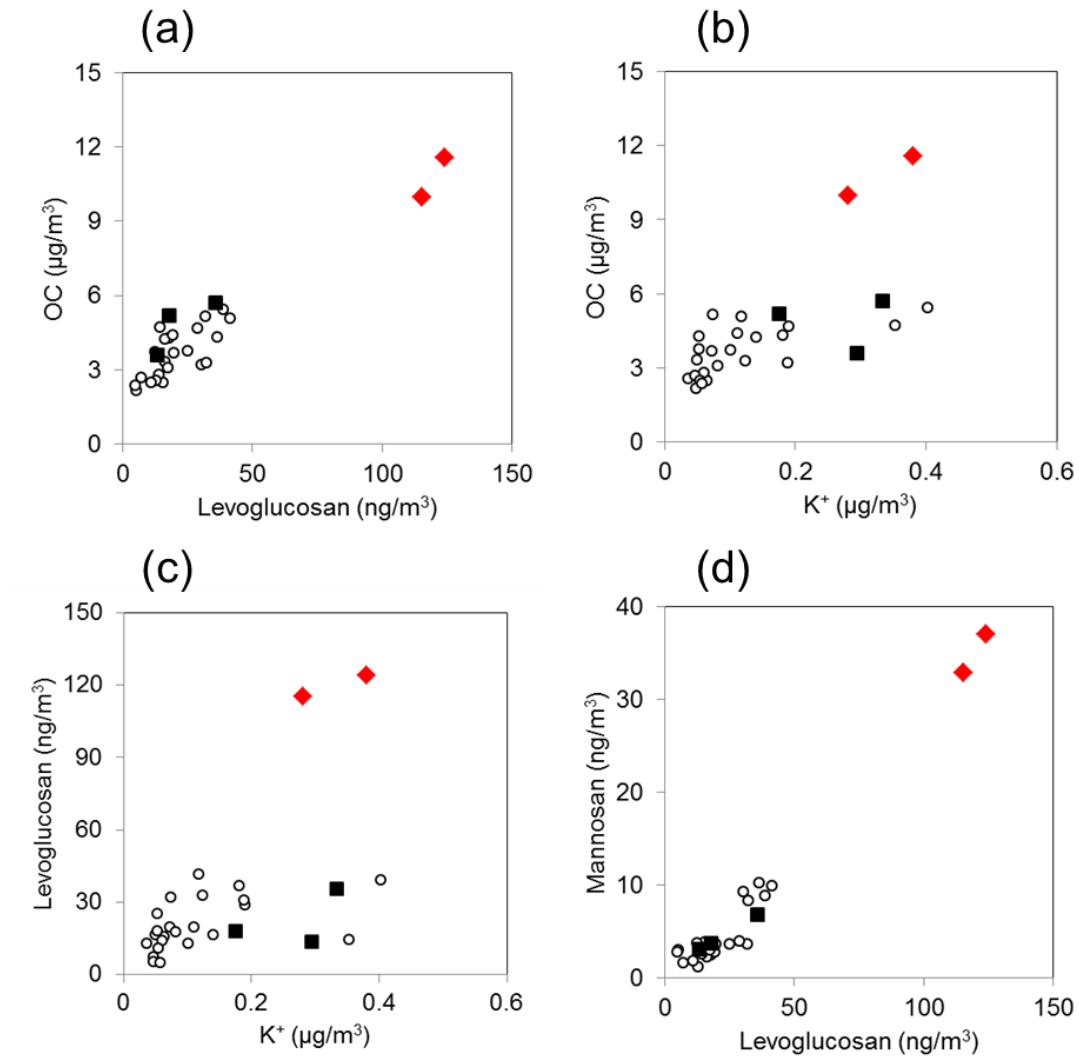
(a)
OC (μg/m3)
Levoglucosan (ng/m3)
(b)
OC (μg/m3)
K+ (μg/m3)
(c)
Levoglucosan (ng/m3)
K+ (μg/m3)
(d)
Mannosan (ng/m3)
Levoglucosan (ng/m3)

Figure 12

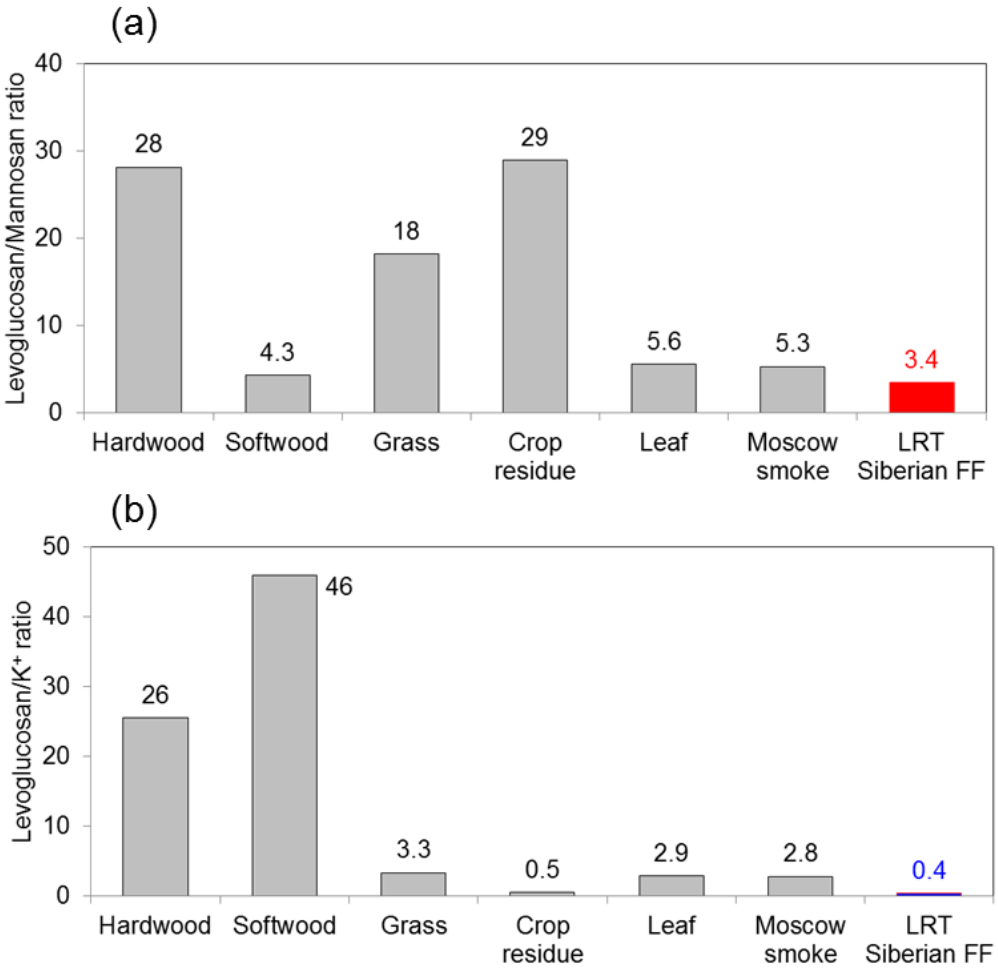
(a)
Levoglucosan/Mannosan ratio
40
30
20
10
0
28
4.3
18
29
5.6
5.3
3.4
Hardwood
Softwood
Grass
Crop residue
Leaf
Moscow smoke
LRT Siberian FF
(b)
Levoglucosan/K+ ratio
50
40
30
20
10
0
26
46
3.3
0.5
2.9
2.8
0.4
Hardwood
Softwood
Grass
Crop residue
Leaf
Moscow smoke
LRT Siberian FF